Egyptian Journal of Radiology and Nuclear Medicine

CASE REPORT Open Access

Imaging case series of melioidosis: the great masquerader

Dhanush Amin[1*], Sridevi Chinta[1], Anu Kapoor[1], M. V. S. Subbalaxmi[2], D. Amulya Reddy[2], A. Neelima[3] and Jyotsna Yarlagadda[1]

Abstract

Background Melioidosis is an infectious disease caused by Gram-negative bacterium *Burkholderia pseudomallei*. It is endemic to Southeast Asia. Inhalation, inoculation and ingestion are major routes of transmission. Increased risk of infection is seen in patients with diabetes, alcoholism, chronic renal and liver failure and malignancy. The aim of the present case series is to describe the varied imaging manifestations of melioidosis.

Case presentation This is a retrospective review of imaging findings in eight patients with culture-proven B. pseudomallei infections diagnosed in our institute from September 2019 to September 2021. A total of eight culture-proven melioidosis cases were reported from our institute. All of them had multiorgan involvement and predisposing conditions or risk factors, most common being diabetes mellitus and alcoholism. Lung was the most common organ involved showing nodules and consolidations followed by liver and spleen demonstrating multiple 'honeycomb'-like abscesses. Musculoskeletal manifestations included osteomyelitis and intramuscular abscess. Cerebral abscess, cerebral infarcts, prostatic abscess, abdominal aortic mycotic aneurysm with periaortic hematoma and splenic vein thrombosis with splenic infarcts were a few other manifestations.

Conclusions Melioidosis is a great mimicker with acute, subacute or chronic clinical course involving multiple organs and resembling other common infections. Hence, it should be considered as a possible etiological agent when evaluating patients with risk factors and multiorgan involvement.

Keywords Abdomen and GIT, Cardiopulmonary, Musculoskeletal, Neuro, Urogenital, Vascular and interventional

Background

Melioidosis is an infectious disease caused by the gram-negative bacterium *Burkholderia pseudomallei*. It is endemic to Southeast Asia, Northern Australia, and parts of Oceania. Inhalation, inoculation of cutaneous abrasions and oral ingestion are the frequent modes of transmission [1]. A large majority of patients have predisposing conditions like diabetes mellitus, alcoholism, chronic renal and liver disease, thalassemia, and malignancy. The spectrum of manifestation ranges from asymptomatic or subclinical to acute and chronic forms. Lung is the most commonly affected organ with multiorgan involvement in a large number of cases. Spleen and liver are the most common abdominal visceral organs involved and are characterized by abscesses with a typical "honeycomb pattern" [2]. Musculoskeletal manifestation includes osteomyelitis, septic arthritis, and soft tissue abscesses. Cultures from blood or infected organs confirm the diagnosis in most cases [3]. In the appropriate clinical setting, radiological imaging and guided

*Correspondence:
Dhanush Amin
amindhanush13@gmail.com
[1] Department of Radiology and Imageology, Nizam's Institute of Medical Sciences, Panjagutta, Hyderabad 500082, Telangana, India
[2] Department of General Medicine, Nizam's Institute of Medical Sciences, Hyderabad, India
[3] Department of Microbiology, Nizam's Institute of Medical Sciences, Hyderabad, India

aspiration play an important role in the early diagnosis and management of melioidosis. The aim of the present case series is to describe the varied imaging manifestations of Melioidosis.

Case presentation

This is a retrospective review of imaging findings in eight patients with culture-proven B. pseudomallei infection diagnosed at our institute (a tertiary care hospital in South India) between September 2019 to September 2021. We present here the spectrum of imaging manifestations in these cases (Table 1).

Table 1 Summary of the imaging manifestations and organ involvement in our case series

	Imaging manifestations
Case 1	Hepatic and splenic abscesses, multiple pulmonary nodules
Case 2	Hepatic, splenic, and prostatic abscesses
Case 3	Calcaneal osteomyelitis with joint effusion, pulmonary consolidation
Case 4	Osteomyelitis of femur with intramuscular abscess
Case 5	Multiple pulmonary nodules with halo sign, brain infarcts
Case 6	Abdominal aortic mycotic aneurysm with periaortic hematoma
Case 7	Hepatic and splenic abscesses, splenic vein thrombosis, and splenic infarct
Case 8	Brain abscesses with pachymeningitis

Case 1

A 22-year-old diabetic male presented with history of high-grade fever, vomiting, and loss of appetite for 2 weeks. Ultrasound of the abdomen revealed multiple anechoic lesions in the liver and spleen. Contrast-enhanced computed tomography (CECT) abdomen (Fig. 1) showed hepatosplenomegaly with multiple hypodense lesions in the liver and spleen showing enhancing internal septations with a honeycomb-like appearance. High-resolution computed tomography (HRCT) chest (Fig. 2) showed multiple nodules in both lungs. Blood culture showed growth of *Burkholderia pseudomallei*.

Case 2

A 28-year-old male with no prior co-morbidities presented with high-grade fever and abdominal pain for 1 month with purulent urethral discharge for one week. CECT abdomen (Fig. 3) showed hepatomegaly with small clusters of peripherally enhancing hypodense lesions in segments II and III with similar lesions in the spleen. Also noted was an enlarged prostate with a small peripherally enhancing hypodense lesion suggestive of prostatic abscess. Ultrasound-guided aspiration and culture from the liver lesion grew *B. pseudomallei*.

Case 3

A 38-year-old diabetic male presented with pain in the left ankle and high-grade fever with chills for 6 days. The

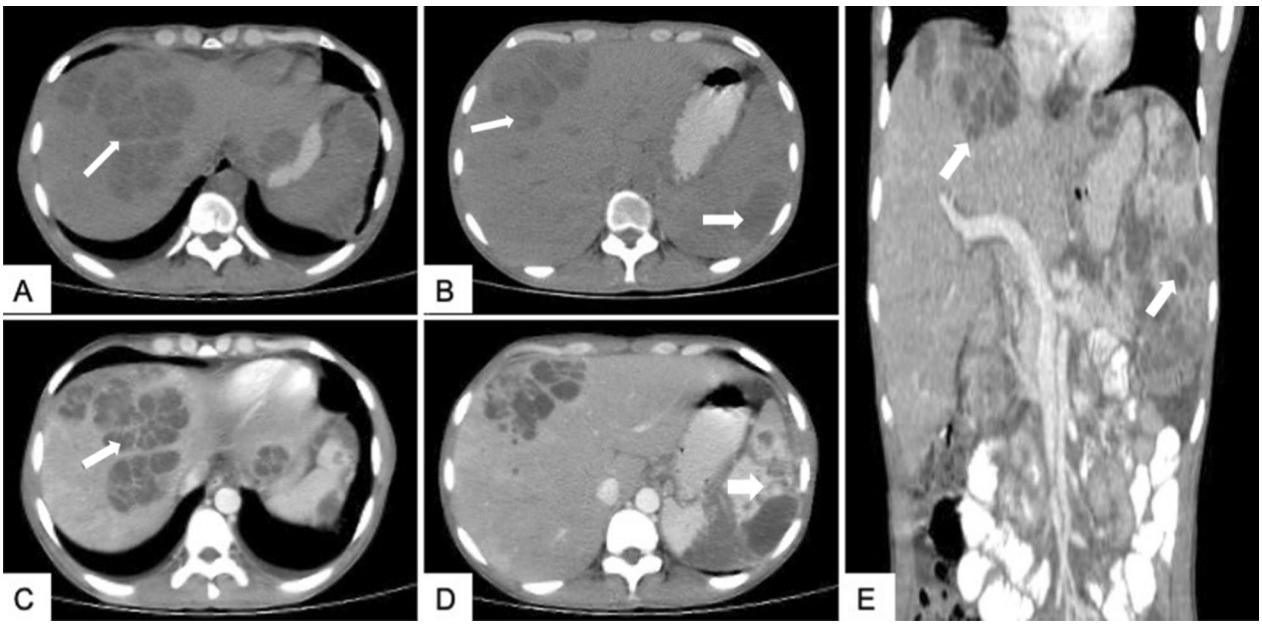

Fig. 1 CT abdomen-Plain **A**, **B** and contrast-enhanced **C**, **D** axial and coronal **E** images showing multiple hypodense lesions in the liver and spleen (arrow) with enhancing internal septations giving a "honeycomb" appearance (arrow)

Fig. 2 HRCT chest–lung window images showing multiple small nodules in both lungs (arrow)

Fig. 3 Contrast-enhanced CT of abdomen **A** & **B** showing multiple irregular honeycomb-like abscesses in liver and spleen (arrows). **C** Axial sections through pelvis show a peripherally enhancing hypodense lesion in the prostate (arrow) suggestive of abscess

radiograph of left ankle (Fig. 4) showed ill-defined lytic lesion in the posterior aspect of the calcaneum. MRI of the left ankle (Fig. 5) showed PD (proton density)/T2 heterogeneously hyperintense lesion in the calcaneum. Minimal effusion was noted in tibiotalar and talocalcaneal joints with imaging features suggestive of osteomyelitis. HRCT chest (Fig. 6) of the patient showed an area of consolidation in the right upper lobe. Blood and pus cultures showed growth of *B. pseudomallei*.

Fig. 4 Lateral radiograph of the ankle showing an ill-defined lytic lesion in the posterior aspect of calcaneum (arrow). A small sclerotic bone island is also noted in the anterior aspect of calcaneum

Case 4

A 43-year-old diabetic male with complaints of pain in the right thigh and fever for 4 months. The radiograph of right thigh (Fig. 7A) showed an area of sclerosis in the diaphysis of the right femur with mild adjacent soft tissue thickening. MRI of the right thigh (Fig. 7B, C) showed features suggestive of osteomyelitis of the femur with multiple abscesses in adjacent muscles. Skeletal scintigraphy (Fig. 7D) showed heterogeneous increased tracer uptake involving the entire right femur. Pus culture from the lesion showed a growth of *B. pseudomallei*.

Case 5

A 25-year-old diabetic male, also a chronic smoker and alcoholic, presented with 3 weeks history of fever, cough with expectoration, shortness of breath and right-sided chest pain. Following this, the patient developed right hemiplegia and was diagnosed to have an acute ischemic stroke. Chest radiograph (Fig. 8) showed multiple alveolo-nodular opacities in both lungs. HRCT Chest (Fig. 9) showed multiple nodules of varying sizes scattered in

Fig. 5 MRI of left ankle—T2W sagittal **A** and proton density (PD) Fat-Sat sagittal **B**, coronal **C** and axial images **D** showing an ill-defined hyperintense lesion in the calcaneum (arrow) with minimal effusion in the talocalcaneal joint—features suggestive of calcaneal osteomyelitis

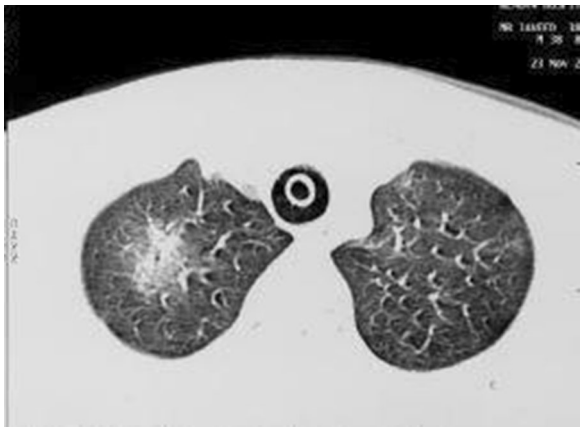

Fig. 6 HRCT chest–lung window image showing an area of consolidation in the right upper lobe

bilateral lung parenchyma, with few of them showing the Computed tomography halo sign. MRI of the brain (Fig. 10) revealed infarcts in the left frontal lobe, left centrum semiovale, left corona radiata, and posterior limb of the left internal capsule. Blood culture showed growth of *B. pseudomallei*.

Case 6

A 55-year-old diabetic male patient presented with fever, abdominal pain and altered mental status for 4 days. Ultrasound abdomen showed mixed echogenicity collection in retroperitoneum surrounding the aorta. CECT abdomen (Fig. 11) showed a Mycotic aneurysm of the infrarenal abdominal aorta. Blood culture revealed growth of *B. pseudomallei*; hence, the diagnosis of melioidosis was established. The patient underwent an aortic bypass graft surgery but unfortunately expired after two days.

Case 7

A 36-year-old diabetic and alcoholic male patient presented with complaints of fever for one month, pain abdomen, and yellowish discoloration of the eyes for 1 week. CECT abdomen (Fig. 12) revealed hepatosplenomegaly with multiple loculated hypodense lesions of varying sizes with peripheral post-contrast enhancement in both lobes of the liver and spleen giving a honeycomb appearance. A filling defect was noted in the splenic vein at the hilum, with a wedge-shaped, non-enhancing hypodense lesion in the spleen suggestive of splenic vein thrombosis with infarct. Ultrasound-guided aspiration of the liver abscess was done which showed growth of *B. pseudomallei*.

Case 8

A 52-year-old diabetic male patient with complaints of right-sided headache for 4 months and fever with chills and visual disturbances for 3 months. Non-contrast computed tomography (NCCT) (Fig. 13) and contrast MRI of the brain were done which showed ill-defined heterogeneously hypodense lesions in right temporal and parieto-occipital lobes. These were hyperintense on T2 with hypointense rim and surrounding vasogenic edema. The lesions were partially suppressed on FLAIR with diffusion restriction and peripheral post-contrast enhancement with adjacent pachymeningeal enhancement. Mass effect is in the form of effacement of adjacent sulci, compression of ipsilateral lateral ventricle, and midline shift toward left. Imaging diagnosis of brain abscess with meningitis was made. Craniotomy and surgical drainage of abscesses were done due to worsening clinical symptoms and poor response to anti-tubercular therapy. However, the patient succumbed a week later. Pus culture revealed growth of *B. pseudomallei*.

Fig. 7 Radiograph of right femur **A** showing sclerosis involving the diaphysis of femur with cortical tunneling and mild adjacent soft tissue component (arrow). STIR (short tau inversion recovery) coronal MR image **B** showing hyperintensities in entire femur and adjacent muscles (arrow). T2W sagittal MR image **C** showing an intramuscular abscess with surrounding edema (arrow). Technetium-99 methylene diphosphonate (Tc-99 MDP) bone scan **D**—3 h delayed image showing diffuse tracer uptake in the entire right femur (arrow)

Fig. 8 Chest radiograph showing multiple alveolo-nodular opacities in both lungs

Discussion

Burkholderia pseudomallei was first recognized by Whitemore and Krishnaswami in Burma in the year 1912 [4]. *B. pseudomallei* is a gram-negative organism that is naturally present in soil and surface groundwater [5]. It possesses multiple virulence factors and a broad spectrum of antibiotic resistance making it highly adaptable and enabling it to produce a variety of non-specific signs and symptoms hindering the diagnosis and management, hence called "the great mimicker" [6]. Routes of transmission are exposure through broken skin, inhalation, and ingestion with certain environmental factors like the rainy season, and occupations like farming are known to increase the risk of exposure [7]. The majority of the immunocompetent individuals have a subclinical disease; only those with acute or chronic clinical symptoms are considered to have melioidosis [6]. Diabetes mellitus is the most common predisposing factor, other known risk factors are male sex, age > 45 years, alcoholism, chronic liver, lung, and kidney diseases, hematological disorders like thalassemia, and immunosuppression and prolonged steroid use. In our case series, seven patients were diabetic.

Lung is the most common organ affected by melioidosis. Radiologically acute pulmonary melioidosis presents with multiple small pulmonary nodules and multi-lobar infiltrates which begin in the upper lobes and progress to cavity and abscess formation [8]. In subacute and chronic forms, mixed nodular and patchy alveolar opacities are seen.

Pulmonary tuberculosis is a differential diagnosis to be considered in these cases, but sparing of lung apex, less fibrosis, absence of pleural effusion with no mediastinal lymphadenopathy, and presence of confluent consolidation go more in favor of melioidosis [9]. Cavities in melioidosis are relatively thin-walled and rarely contain air-fluid levels, differentiating it from

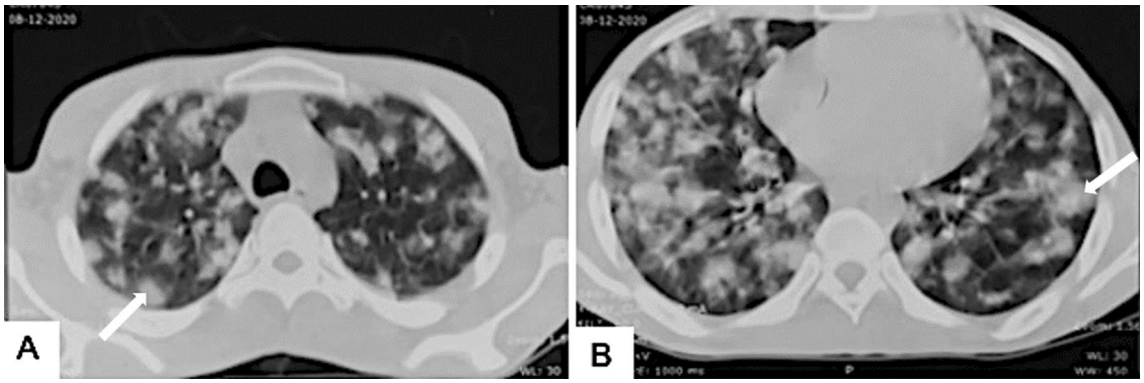

Fig. 9 CT chest–lung window images **A**, **B** showing multiple nodules of varying sizes scattered throughout the lung parenchyma, some of which are surrounded by ground glass density (arrows)

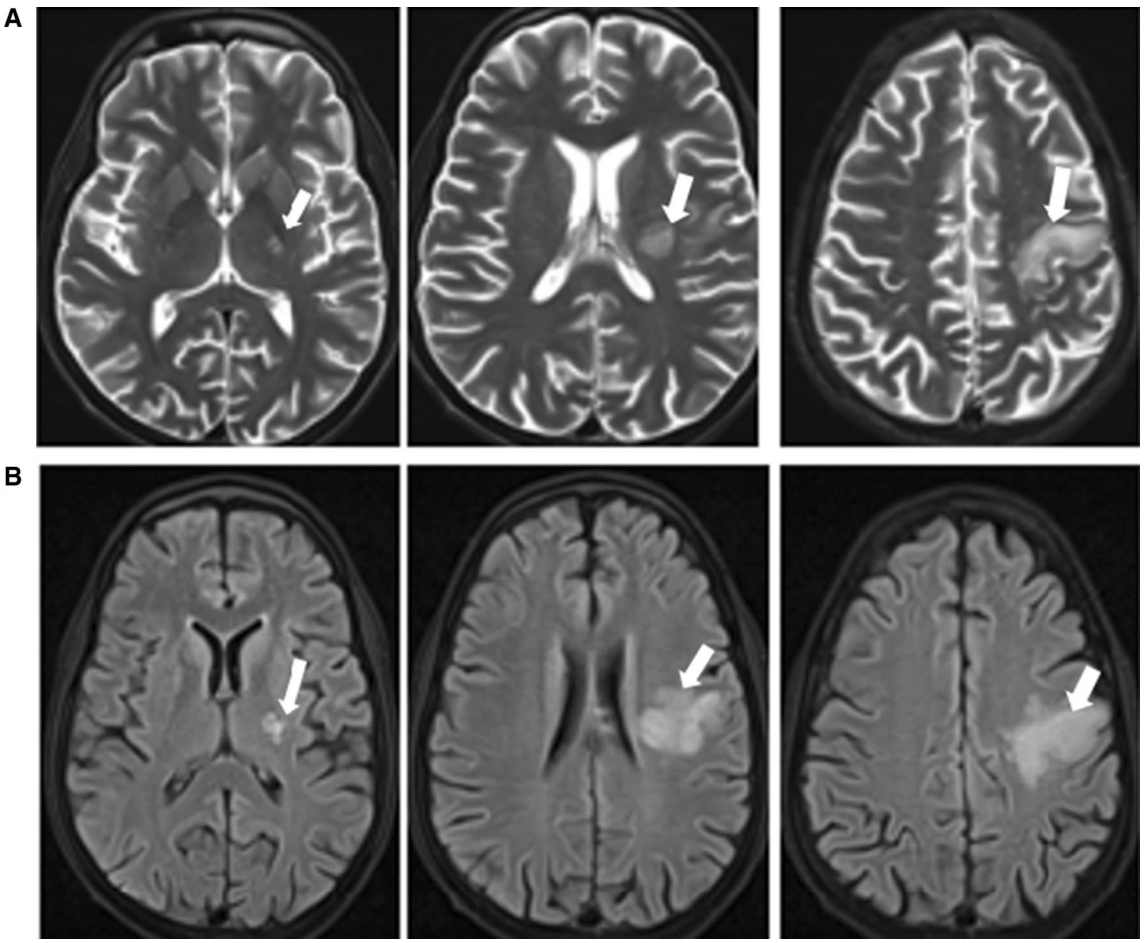

Fig. 10 **A** T2 and **B** Flair axial sections of MR Brain showing hyperintensities in left thalamus, left corona radiata and centrum semiovale suggestive of infarcts (arrow)

Staphylococcus aureus. In our case series, imaging differential of angio-invasive fungal infection or granulomatosis with polyangiitis was initially considered; however, the absence of paranasal sinuses and upper respiratory tract involvement made this a less likely possibility.

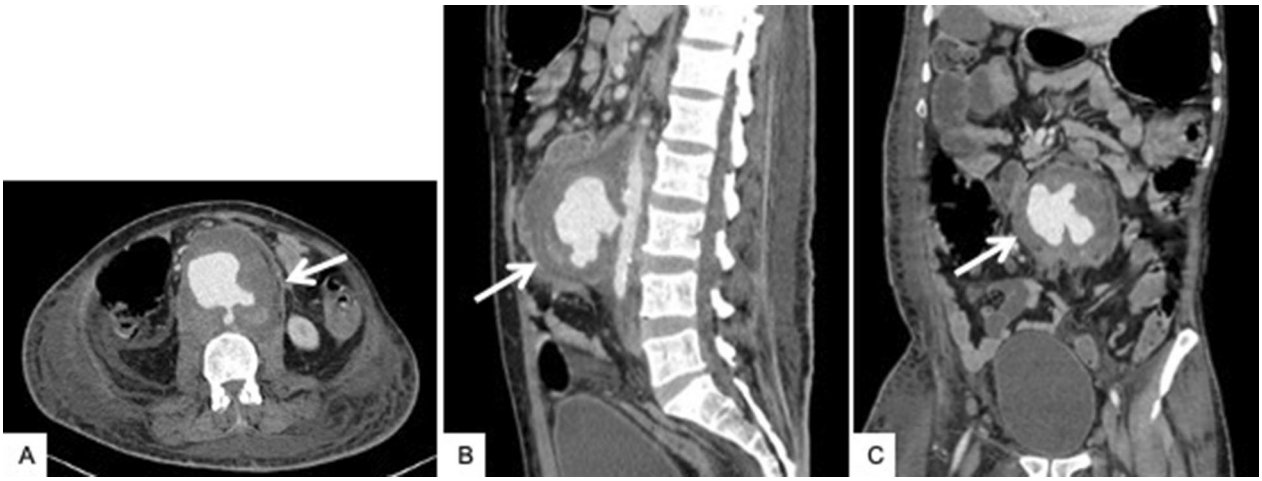

Fig. 11 CECT abdomen–axial **A**, sagittal **B** and coronal **C** reformatted images showing a large irregular partially thrombosed pseudoaneurysm (arrow) arising from the infra renal abdominal aorta

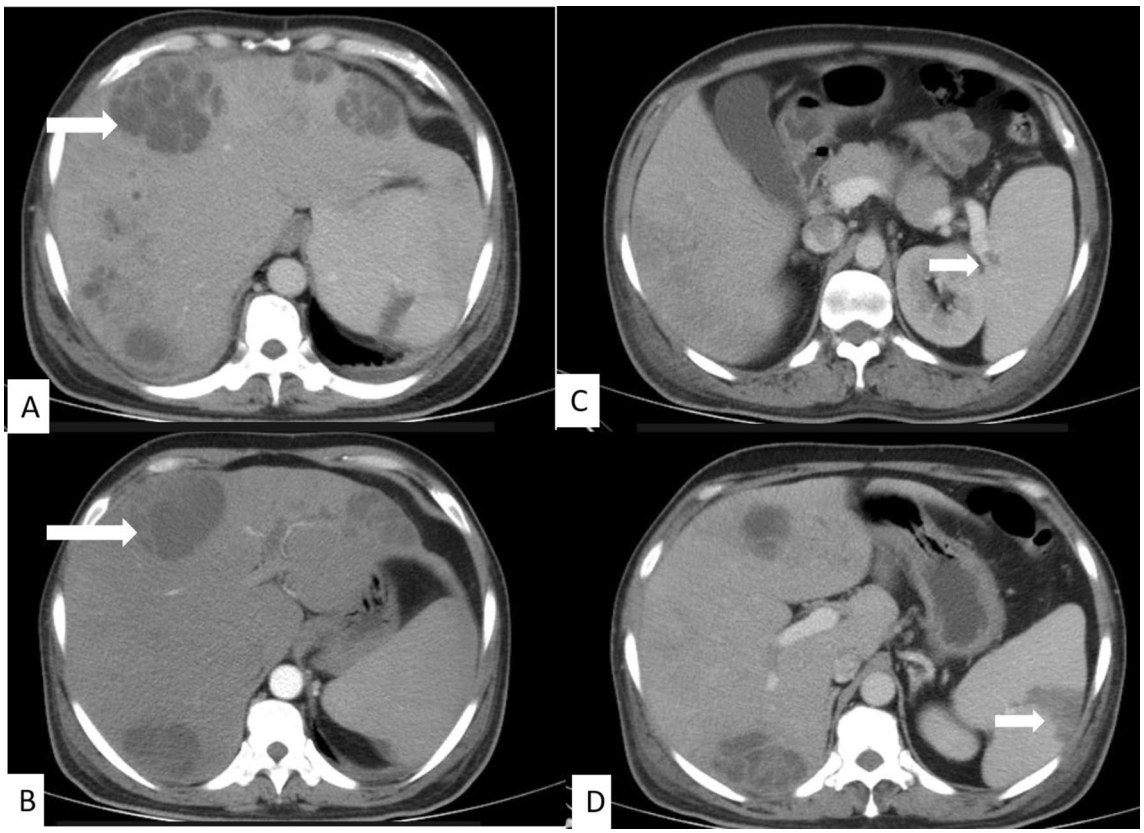

Fig. 12 Contrast-enhanced CT of the abdomen-venous **A** and arterial **B** phase axial images showing multiple peripherally enhancing hypodense lesions with internal septations giving honeycomb appearance in the liver (arrows). Venous phase axial images **C** & **D** show a filling defect (thrombus) in splenic vein at the splenic hilum (small arrow) and a wedge-shaped peripheral non-enhancing hypodense lesion in spleen suggestive of splenic infarct (small arrow)

Spleen is the most common abdominal visceral organ involved, followed by the liver and kidney [10]. Liver and splenic abscesses in melioidosis are seen as single or multiple multiloculated lesions described as 'honeycomb' or 'string of pearls' sign [11]. Liver and splenic abscesses are also caused by other organisms like *Candida albicans*,

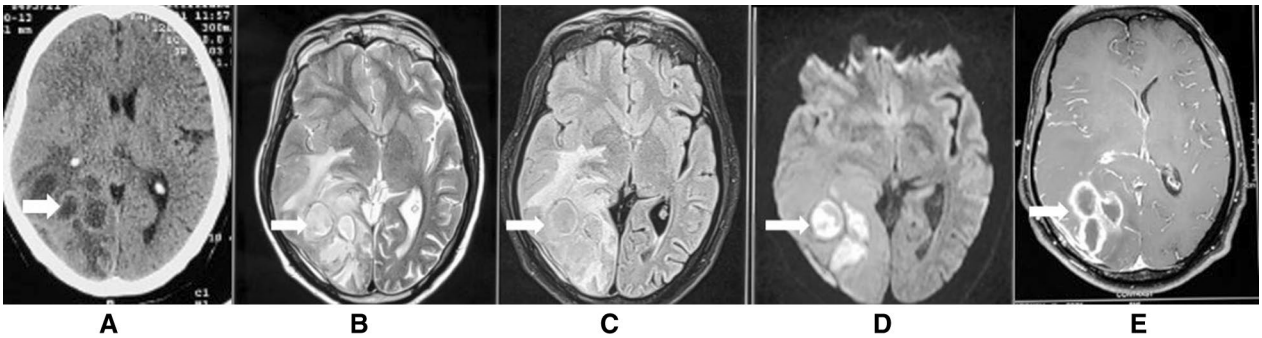

Fig. 13 **A** NCCT brain showing ill-defined hypodense lesions in right occipital location (arrow). **B** T2W and **C** FLAIR MR images showing T2 hyperintense lesions with surrounding vasogenic edema not suppressed in FLAIR images(arrow) **D** DWI image showing diffusion restriction (arrow). Post-contrast images **E** showing peripherally enhancing lesions with adjacent pachymeningeal enhancement (arrow)—suggestive of brain abscesses with pachymeningitis

Mycobacterium tuberculosis, and Mycobacterium avium intercellular with an overlap of imaging features [12].

The presence of hepatic and splenic abscess together is highly suggestive of melioidosis, especially in patients with co-morbidities or with history of travel to endemic areas [10].

Systemic melioidosis is a pro-inflammatory condition due to depletion of antithrombin, protein C, and protein S leading to a thrombotic state [13]. In one of our cases, splenic vein thrombosis with splenic infarcts was also noted.

Prostatic involvement is one of the rarer manifestations of melioidosis. The infection may present as prostatic abscess predominantly involving the peripheral zone [14].

Neurological manifestations of melioidosis are rare. The spectrum of findings includes brain parenchymal disease which can present as micro or macro-abscesses with features of encephalitis. In our case, macro-abscesses were noted in the brain parenchyma with adjacent pachymeningitis. Involvement of bony calvarium and soft tissues of the scalp may also be seen.

The prevalence of musculoskeletal involvement by melioidosis ranges from 5 to 48% in different regions of the world [15]. The spectrum varies from osteomyelitis, septic arthritis, synovitis to soft tissue abscesses. In our series, involvement of calcaneum and femur with features of osteomyelitis and soft tissue abscesses was noted in two cases. These imaging features are non-specific and cannot be differentiated from other etiological agents.

Mycotic aneurysms are documented but a very rare manifestation of melioidosis and is seen in only 1% of affected patients [15]. It is caused by seeding of already damaged atherosclerotic vessels which is likely to be the etiology in our case too.

Conclusions

As observed in literature and our case series, melioidosis is truly a great masquerader involving multiple organs and mimicking other common infective conditions. Awareness of the imaging manifestation of melioidosis is therefore important and should be considered as a possible cause of infection in an appropriate clinical setting. Early diagnosis of this uncommon infection will aid in the appropriate management of these patients.

Abbreviations

B. pseudomallei	Burkholderia pseudomallei
CECT	Contrast-enhanced computed tomography
HRCT	High-resolution computed tomography
PD	Proton density
STIR	Short tau inversion recovery
MR	Magnetic resonance
Tc 99 MDP	Technicium 99 methylene diphosphonate
CT	Computed tomography
NCCT	Non-contrast computed tomography
FLAIR	Fluid-attenuated inversion recovery
DWI	Diffusion-weighted imaging

Acknowledgements

Not applicable.

Author contributions

DA contributed to conception, collection of data, drafting and approval of the submitted work. SC collected the data, drafted and approved the submitted work. AK contributed to conception, interpretation, approval of the submitted work, and revision of the draft. MVSS provided clinical data and approved the submitted work. DAR provided clinical data and approved the submitted work. AN provided clinical data and approved the submitted work. JY contributed to interpretation, approval of the submitted work, and revision of the draft. All authors read and approved the final manuscript.

Funding

Not applicable.

Availability of data and materials

The datasets used and /or analyzed during the current series are available from the corresponding author on reasonable request.

Declarations

Ethics approval and consent to participate
Ethics approval was waived off. All patients included in the series gave written informed consent to participate in this series.

Consent for publication
All patients included in this series gave written informed consent to publish the data contained within this series.

Competing interests
The authors declare that they have no competing interests.

Received: 18 August 2022 Accepted: 17 February 2023
Published online: 27 February 2023

References

1. Patil S, Gondhali G (2021) Pulmonary melioidosis masquerading as tuberculosis: a case report. Electron J Gen Med 18(5):em310
2. Ong SC, Alemam MM, Zakaria NA, Halim NA (2017) Honeycomb and necklace signs in liver abscesses secondary to melioidosis. Case Rep 2017:bdcr-2017
3. Ashdown LR (1979) An improved screening technique for isolation of Pseudomonas pseudomallei from clinical specimens. Pathology 11(2):293–297
4. Whitmore AK, Krishnaswami CS (1912) A hitherto undescribed infective disease in Rangoon. Indian Med Gazette 47(7):262
5. Limmathurotsakul D, Golding N, Dance DA, Messina JP, Pigott DM, Moyes CL, Rolim DB, Bertherat E, Day NP, Peacock SJ, Hay SI (2016) Predicted global distribution of Burkholderiapseudomallei and burden of melioidosis. Nat Microbiol 1(1):1–5
6. Wiersinga WJ, Virk HS, Torres AG, Currie BJ, Peacock SJ, Dance DA, Limmathurotsakul D (2018) Melioidosis. Nat Rev Dis Primers 4(1):1–22
7. Cheng AC, Currie BJ (2005) Melioidosis: epidemiology, pathophysiology, and management. Clin Microbiol Rev 18(2):383–416
8. Dhiensiri TU, Puapairoj SO, Susaengrat WA (1988) Pulmonary melioidosis: clinical-radiologic correlation in 183 cases in northeastern Thailand. Radiology 166(3):711–715
9. Lim KS, Chong VH (2010) Radiological manifestations of melioidosis. Clin Radiol 65(1):66–72
10. Tan AP, Pui MH, Tan LK (1995) Imaging patterns in melioidosis. Australas Radiol 39(3):260–264
11. Ong SC, Alemam MM, Zakaria NA, Halim NA (2017) Honeycomb and necklace signs in liver abscesses secondary to melioidosis. Case Rep 2017:bcr-2017
12. Wilde CC, Kueh YK (1991) Case report: tuberculous hepatic and splenic abscess. Clin Radiol 43(3):215–216
13. LaRosa SP, Opal SM, Utterback B, Yan SC, Helterbrand J, Simpson AJ, Chaowagul W, White NJ, Fisher CJ Jr (2006) Decreased protein C, protein S, and antithrombin levels are predictive of poor outcomes in Gram-negative sepsis caused by Burkholderia pseudomallei. Int J Infect Dis 10(1):25–31
14. Morse LP, Moller CC, Harvey E, Ward L, Cheng AC, Carson PJ, Currie BJ (2009) Prostatic abscess due to Burkholderia pseudomallei: 81 cases from a 19-year prospective melioidosis study. J Urol 182(2):542–547
15. Currie BJ, Fisher DA, Howard DM, Burrow JN, Lo D, Selva-Nayagam S, Anstey NM, Huffam SE, Snelling PL, Marks PJ, Stephens DP (2000) Endemic melioidosis in tropical northern Australia: a 10-year prospective study and review of the literature. Clin Infect Dis 31(4):981–986

Publisher's Note